Control of Peptide Secondary Structure and Dynamics in Poly(γ-benzyl-L-glutamate)-*b*-polyalanine Peptides

A. Gitsas,[†] G. Floudas,*[,†] M. Mondeshki,[‡] H. W. Spiess,[‡] T. Aliferis,[§] H. Iatrou,[§] and N. Hadjichristidis[§]

Department of Physics, University of Ioannina, and Foundation for Research and Technology-Hellas (FORTH), Biomedical Research Institute (BRI), P.O. Box 1186, GR-45110 Ioannina, Greece, Max-Planck-Institut für Polymerforschung, D-55021 Mainz, Germany, and Department of Chemistry, University of Athens, Panepistimiopolis, Zografou, GR-15771 Athens, Greece

Received August 4, 2008; Revised Manuscript Received September 10, 2008

ABSTRACT: The stability, persistence and dynamics of the peptide secondary motifs are investigated in a series of poly(γ-benzyl-L-glutamate)-*b*-polyalanine (PBLG-*b*-PAla) polypeptides through a combination of structural (X-rays, NMR) and dynamic (Dielectric Spectroscopy, NMR) probes. The unfavorable enthalpic interactions between the unlike blocks give rise to nanophase separation that results in the destabilization of PAla β-sheets. Contrary to this, the overall helicity of PBLG α-helices is enhanced. The dynamics of the "defected" amorphous segments and of the more ordered segments are studied by DS and ^{13}C NMR, respectively. These probes provide information on the time scale and the mechanism of molecular and supramolecular motion.

Introduction

Nature employs simple and elegant molecular tools and mechanisms to synthesize soft and hard tissues with unique properties and functions. Of key importance in this process of molecular engineering is the combination of building blocks with controlled self-assembly in a hierarchical manner from the nano- to the macroscale. In this process, proteins and polypeptides are employed as the main molecular building blocks that combine the ability to self-assemble with molecular recognition and genetic manipulation.[1,2]

Polypeptides form hierarchically ordered structures with α-helices and β-strands being the fundamental secondary motifs. The α-helical motif, stabilized by intramolecular hydrogen bonds, has been the most studied secondary motif due to its high frequency in naturally occurring proteins. It is thought that understanding the dynamics of helix formation can lead to greater insight in the protein folding problem. The α-helix dipole, in particular, has its origin on the single peptide unit with a dipole moment of ∼3.4 D. In a perfect α-helix, the peptide dipole moments are aligned parallel to the helix axis resulting in a macro-dipole that runs from the C-terminal end to the N-terminal end.[3] Chimeric protein design[4] through capping residues can further enhance the helicity; for example, N-terminal cysteine capping of alanine peptides enhance their overall helicity and even allow the helix to persist at temperatures above denaturation.[5] From the synthetic point, the most well-known example of an α-helical polypeptide is poly(γ-benzyl-L-glutamate) (**PBLG**) that has been employed as a model rigid-rod polymer.[6,7] Recent developments, however, mainly through dielectric spectroscopy (DS), revealed that the polypeptide backbone contains several amorphous "defects" giving rise to helical segments of rather low persistence.[8,9] These "defects" are responsible for the dynamic arrest at the liquid-to-glass transition, a phenomenon that is independent of the peptide secondary structure and the presence or absence of side-groups.[10]

The secondary motif of β-sheets is also very important; for example, insoluble β-sheet aggregates are associated with the development of a number of neurodegenerative disorders such as Alzheimer's and prion diseases. In this respect, polyalanine-based peptides have been proposed as soluble model systems for self-associated β-pleated sheet complexes.[11] Polyalanine (**PAla**) plays also a vital role in silk proteins, i.e., proteins composed of repetitive sequences containing smaller motifs or blocks. An example of a silk protein is the spider silk (dragline silk), well-known for its exceptional mechanical properties. This filament consists of two distinct proteins known as major ampullate spidroins 1 and 2 (MaSp1 and MaSp2) that are composed of crystalline polyalanine-rich β-sheets embedded into glycine-rich regions.[12] The above examples show that PAla can take part in both secondary motifs.

Work on biomimetic materials[13] has progressed quickly over the past decade, partially thanks to the advances in the synthesis of polypeptides and copolypeptides. Conformational studies of model polypeptides are an important step toward mimicking the biological activity of more complex proteins. Therefore block copolypeptides can be employed as model systems[8−10,14−23] that follow nature's strategies for producing supramolecular bioactive assemblies with potential applications in tissue engineering and drug delivery.[24] Other studies investigated the effect of chain topology on the peptide secondary structures.[25−28] A recent study of block copolypeptides[21] composed from an α-helical polypeptide (PBLG) and a solely β-sheet forming peptide (polyglycine, PGly) revealed that the disparity in the packing efficiency of the two peptides induced multiple chain folding of the PGly backbone. Copolypeptides of particular interest are ones composed of both α-helical and β-sheet motifs. In such systems, both secondary motifs are exposed to the same thermodynamic field created by the block copolymer nature and this allows studying their stability and persistence. In this respect, PAla, possessing both secondary motifs is an ideal candidate as one of the blocks.[29−31]

In the present study we report on the self-assembly and dynamics of a series of model PBLG-*b*-PAla copolypeptides aiming at exploring the effect of thermodynamic field on the stability and persistence of the α-helical and β-sheet motifs as well as the associated dynamic changes within the copolymer nanodomains. For this purpose we combine thermal and

* Corresponding author.
[†] Department of Physics, University of Ioannina, and Foundation for Research and Technology-Hellas (FORTH), Biomedical Research Institute (BRI).
[‡] Max-Planck-Institut für Polymerforschung.
[§] Department of Chemistry, University of Athens.

10.1021/ma801770b CCC: $40.75
Published on Web 10/16/2008

Table 1. Molecular Characteristics of the Polymers

compound	polyalanine (%)[a]	M_w^{total} (g/mol)	M_w^{PBLG} (g/mol)[b]	DP^{PBLG} [d]	M_w^{PAla} (g/mol)[e]	DP^{PAla} [d]	I[b]
$PBLG_{91}$	0		19900[c]	91			1.06
$PBLG_{104}$-*b*-$PAla_{24}$	8.4	24700	22700	104	2000	24	1.08
$PBLG_{115}$-*b*-$PAla_{48}$	16	29400	25100	115	4300	48	1.09
$PBLG_{105}$-*b*-$PAla_{79}$	21	30000	23000	105	7000	79	1.08
$PAla_{107}$	100				9500	107	

[a] Obtained by thermogravimetric analysis (TGA). [b] Obtained by size exclusion chromatography (SEC) in DMF/0.1 N LiBr at 60 °C. [c] Obtained by two-angle laser light scattering SEC (SEC−TALLS). [d] Degree of polymerization. [e] Stoichiometric molecular weights.

structural techniques (DSC, X-ray scattering, NMR) with dynamic probes (dielectric spectroscopy and NMR) that provide a specific picture of the self-assembly. We find that the strong thermodynamic field has consequences on the stability and persistence of the peptide secondary structures. Furthermore the combined dynamic probes provide the time scale and the corresponding geometry of molecular and supramolecular motions.

Experimental Part

Synthesis of Poly(benzyl-L-glutamate-*b*-alanine). *Materials.* The polymerization solvent, DMF (Aldrich, 99.9+ %) was a special grade for peptide synthesis (active impurities <50 ppm) and was further purified by short-path fractional distillation, on the vacuum line, in a custom-made apparatus. The middle fraction was always used. Ethyl acetate, was dried over CaH_2. *n*-Hexane was dried overnight over CaH_2 and then distilled into a flask containing *n*-BuLi. Acetonitrile (Aldrich 99.9%) was dried over phosphorus pentoxide and then fractionally distilled prior to use. *n*-Hexylamine (Aldrich, 99.9%), the initiator, a highly hygroscopic compound, was left to dry over a sodium mirror for 24 h. Then it was diluted with purified DMF, subdivided into ampoules, and stored under high vacuum at room temperature.

Synthesis of NCAs. The NCAs of γ-benzyl-L-glutamate (Glu-NCA) was synthesized from the corresponding α-amino acid and triphosgene in ethyl acetate at 70 °C, under inert atmosphere, according to the literature.[32] The unreacted species along with the HCl and the amino acid salts were removed by extraction with an aqueous alkali solution and water. The organic phase was introduced into a specially designed homemade apparatus for extreme purification by three times crystallization with ethyl acetate and *n*-hexane under high vacuum conditions. Finally the pure NCA was diluted with purified DMF, subdivided into ampoules, and stored under high vacuum at −20 °C. Details are given elsewhere.[33] In the case of Ala-NCA a slightly different procedure was followed. In this case acetonitrile was used as the solvent instead of ethyl acetate. Then, the Ala-NCA was dissolved and dried several times with ethyl acetate under high vacuum, in order to remove the excess triphosgene, along with the remaining HCl. Finally, it was dissolved in ethyl acetate, and was recrystallized from *n*-hexane three times. The purified NCA was diluted in DMF in an apparatus equipped with calibrated ampoules, and stored at −20 °C.

Synthesis of PBLG-b-PAla. A homemade glass apparatus was used without ground joins in order to create and maintain the conditions necessary for the living polymerization of NCAs. The polymerization reactors were designed to have a volume at least three times larger than the volume of the CO_2 generated by each polymerization. The combination of high vacuum and large volume, forces the polymerization to completion. Polymerizations were carried out with *n*-hexylamine as the initiator. After complete consumption of Glu-NCA (2−3 days), a small aliquot was removed from the reactor for characterization, followed by the addition of the second monomer Ala-NCA. The polyalanine block is soluble only in water, and therefore the synthesized copolypeptides formed a gel in DMF. The polymerization was left to completion for one week, and a 5-fold amount (in relation to the DMF) of diethyl ether was added. The final copolypeptides were filtered and dried to constant weight. The PBLG precursors were characterized by SEC, combined with a two-angle LALLS and UV detectors. The instrument was operating at 60 °C with a 0.1N LiBr solution of DMF as a carrier solvent for the determination of the polydispersity index (I) and the number average molecular weight (M_n) of the samples. Complete consumption of the first monomer was verified by the absence of the monomer peak in the SEC-UV chromatograms. Since the copolypeptides could not be characterized by SEC in DMF, their composition was obtained from thermogravimetric analysis (TGA) measurements. The decomposition of PBLG starts at 251 °C, while of PAla at 355 °C, allowing the determination of the weight of each block in the block copolypeptide. The obtained values are given in Table 1, along with the stoichiometric ones. The results shows that the stoichiometric and obtained from TGA composition are close, indicating a high degree of molecular and compositional homogeneity.

Solid-State NMR. The solid state NMR experiments were performed on a Bruker Avance spectrometer with a ^1H frequency of 500.1 MHz and ^{13}C frequency of 125.76 MHz. A Bruker double resonance probe, supporting rotors of 2.5 mm outer diameter at a spinning frequency of 20 kHz, was used in all cases. At high spinning frequencies, additional heating effects caused by bearing gas friction become significant. The sample temperatures given in this article have been corrected for these frictional heating effects following a well-known procedure.[34] For all variable temperature (VT) solid state ^{13}C cross-polarization (CP) magic angle spinning (MAS) NMR experiments an initial 90° pulse with 2.5 μs length and 2 s recycle delay were used. The duration of the a variable amplitude contact pulse (80−100%)[35] was 1 ms and two-pulse phase-modulation (TPPM) ^1H decoupling scheme[36] was used while acquiring the ^{13}C signal. One thousand transients were averaged for the experiments.

X-ray Scattering. Both wide-angle and small-angle X-ray scattering (WAXS/SAXS) measurements have been performed from macroscopically oriented filaments[37] with a diameter of 0.5 mm using a pinhole collimator and a two-dimensional detector (Bruker) with 1024 × 1024 pixels. The extrusion temperatures were 353, 413, and 463 K for **$PBLG_{104}$-*b*-$PAla_{24}$**, **$PBLG_{115}$-*b*-$PAla_{48}$**, and **$PBLG_{105}$-*b*-$PAla_{79}$**, respectively. The PAla homopolypeptide was measured in powder form, since it was impossible to extrude. A graphite monochromator was used (λ=0.154 nm), and the sample-to-detector distance was 7.05 cm. Measurements were made at 303, 353, 393 and 433 K on heating. The recorded 2-D scattered intensities were investigated over the azimuthal angle and are presented as a function of the scattering wave vector q ($q = (4\pi/\lambda)\sin(2\theta/2)$, where 2θ is the scattering angle). Better images were obtained at the highest temperature (433 K) following annealing for ∼12 h. In the SAXS measurements, the sample-to-detector distance was set at 1.8 m. 2-D images were obtained for different temperatures in the range $303 < T < 433$ K in 10 K intervals.

Differential Scanning Calorimetry (DSC). A Mettler Toledo star differential scanning calorimeter was used for the thermal analysis. The copolypeptides were first heated at a rate of 10 K/min to 543 K and subsequently cooled to 123 K with 10 K/min. A second heating run, with the same rate, was used to identify the glass temperature, T_g, and the width of the transition, ΔT_g. The DSC traces, starting with pure PBLG and increasing PAla content, are displayed in Figure 1. As has been discussed earlier,[8−10] the step-like change in the heat flow of **$PBLG_{91}$** associates with the glass temperature originating from amorphous-like segments. In the copolymers a similar step is observed over the same temperature range, although it broadens considerably. An additional small step is evident at T∼470 K in two of the copolymers in the range where

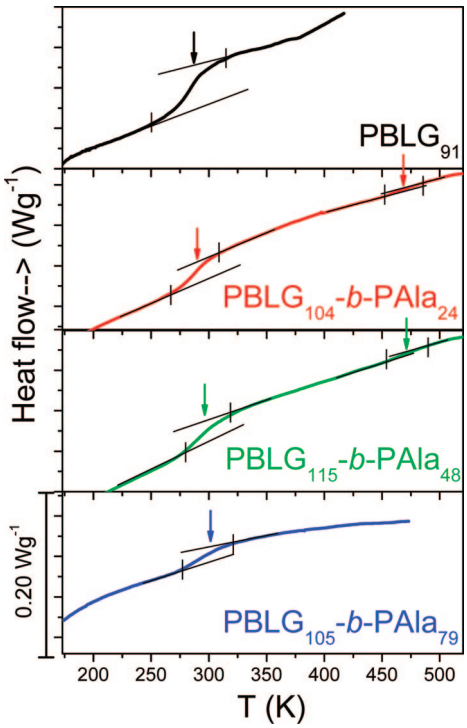

Figure 1. DSC thermograms obtained during the second cooling run (rate 10 K/min). The glass temperature of PBLG (T_g^{PBLG}) shifts to slightly higher temperatures and broadens with increasing PAla composition in the diblocks.

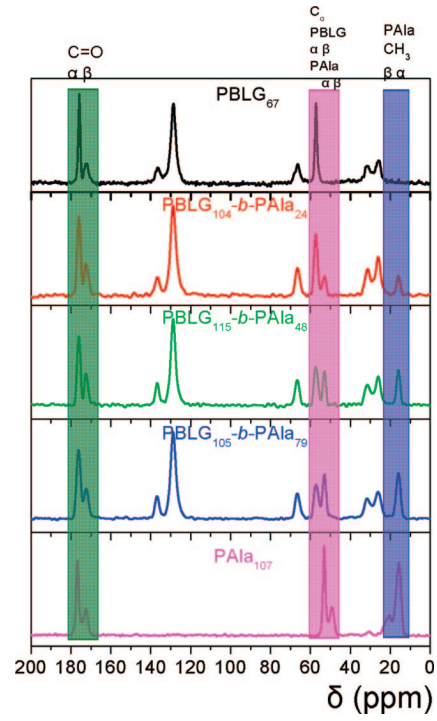

Figure 2. ^{13}C NMR profiles for the **PBLG$_{67}$** and **PAla$_{107}$** homopolypeptides and the copolypeptides. For PBLG$_{67}$ the intense peaks at $\delta_{\approx}$176 and 57.5 ppm arise from the amide C═O and C_α carbon, respectively, and indicate the formation of α-helical secondary structure. On the other hand, the PAla profile exhibits two C_α resonances at $\delta_{\approx}$53.1 and 49.4 ppm, reflecting α-helical and β-sheet conformations, respectively. In the copolymers two C_α resonances are present, at 57.5 ppm and 53.1 ppm, revealing that both blocks form solely α-helical structures.

the T_g^{PAla} is expected. The low temperature step in the specific heat capacity, Δc_p, is equal to 0.40, 0.31, 0.30 and 0.24 J/gK for **PBLG$_{91}$**, **PBLG$_{104}$-*b*-PAla$_{24}$**, **PBLG$_{115}$-*b*-PAla$_{48}$** and **PBLG$_{105}$-*b*-PAla$_{79}$**, respectively, whereas for the high temperature step (T_g^{PAla}) Δc_p = 0.12 and 0.10 J/gK for **PBLG$_{104}$-*b*-PAla$_{24}$** and **PBLG$_{115}$-*b*-PAla$_{48}$**, respectively.

Dielectric Spectroscopy (DS). The dielectric measurements were performed at different temperatures in the range 123−473 K, at atmospheric pressure, and for frequencies in the range from 10^{-2} to 10^6 Hz using a Novocontrol BDS system composed of a frequency response analyzer (Solartron Schlumberger FRA 1260) and a broadband dielectric converter. The sample cell consisted of two electrodes 20 mm in diameter and the sample with a thickness of about 50 μm (due to the high rigidity of the copolymers Teflon spacers were not necessary; the sample thickness was measured before and after the experiment and found to be unchanged). The complex dielectric permittivity $\epsilon^* = \epsilon' - i\epsilon''$, where ϵ' is the real and ϵ'' is the imaginary part, is generally a function of frequency ω, temperature T, and pressure P, although here only the frequency and temperature dependencies have been investigated. [38]There are two principal mechanisms that contribute to ϵ^* in our case: orientation polarization of permanent dipoles (ϵ^*_{dip}) and conductivity contribution (ϵ^*_{cond}) as:

$$\varepsilon^*(\omega,T,P) = \varepsilon^*_{dip}(\omega,T,P) - i\frac{\sigma(T,P)}{\varepsilon_f \omega} \quad (1)$$

where σ is the dc conductivity and ϵ_f the permittivity of free space (=8.854 pF/m). The orientational contribution was fitted using the empirical equation of Havriliak and Negami:[39]

$$\varepsilon^*_{dip}(\omega,T,P) = \varepsilon_\infty(T,P) + \sum_{k=1}^{2} \frac{\Delta\varepsilon_k(T,P)}{[1+(i\omega\tau_{HN}(T,P)^{m_k}]^{n_k}} \quad (2)$$

where $\Delta\epsilon_k(T,P)$ is the relaxation strength of the process under investigation, τ_{HN} is the relaxation time of the equation and m, n ($0 < m$, $mn \leq 1$) describe the symmetrical and asymmetrical broadening of the distribution of relaxation times and $\epsilon_\infty(T,P)$ is the dielectric permittivity at the limit of high frequencies. The relaxation times at maximum loss (τ_{max}) are presented herein and have been analytically obtained by the Havriliak−Negami equation as follows:

$$\left[\sin\left(\frac{\pi m}{2+2n}\right)\right]^{1/m}\tau_{max} = \tau_{HN}\left[\sin\left(\frac{\pi mn}{2+2n}\right)\right]^{1/m} \quad (3)$$

At lower frequencies, ϵ'' rises due to the conductivity ($\epsilon'' = \sigma/(\omega\epsilon_f)$,). The measured ϵ'' spectra have been used for the analysis except at high temperatures where the derivative of ϵ' has been employed ($d\epsilon'/d(\ln\omega) \sim -(2/\pi)\epsilon''$). Since ϵ' is not affected by the conductivity, this method is useful in fitting relaxation processes which are hidden under the conductivity, provided that the system is free of surface polarization effects. Therefore the latter representation was employed in the analysis of the slower process (see Figure 4, below).

Results and Discussion

Supramolecular Structure. The peptide local conformation is conveniently encoded in the ^{13}C chemical shifts[40] hence the polypeptide secondary structure can be identified using ^{13}C cross-polarization-magic angle spinning (CP-MAS) solid state NMR. In Figure 2 characteristic spectra of ^{13}C NMR of both homopolypeptides and of the copolymers are shown. PBLG of high molecular weight (DP > 18) is known to form α-helices.[9] Indeed, the intense resonances at $\delta \approx 176$ and 57.5 ppm arise from the amide C═O and C_α carbon, respectively, and indicate the formation of an α-helical secondary structure. On the other hand, the **PAla$_{107}$** trace exhibits two C_α resonances at $\delta \approx 53.1$ and 49.4 ppm, reflecting α-helical and β-sheet conformations, respectively. The ratio of α-helices to β-sheets amounts to 66:34, where the ratios as obtained from the different groups vary between 63:37 and 69:31.

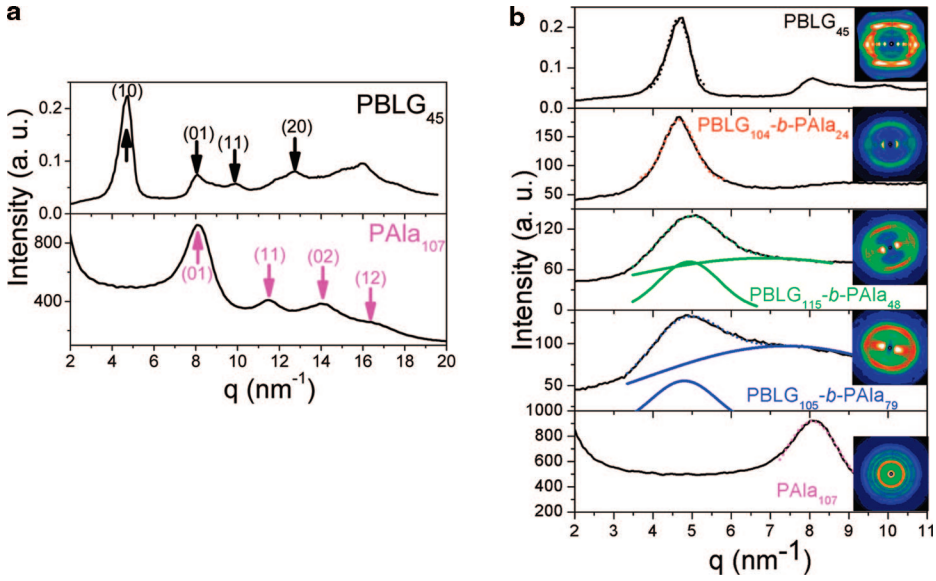

Figure 3. (a) Equatorial WAXS intensity distributions of PBLG and PAla homopolypeptides. The arrows indicate the primary reflections from the hexagonal and orthorhombic unit cells of **PBLG$_{45}$** and **PAla$_{107}$**, respectively. (b) Respective equatorial intensity distributions of the homopolypeptides and the copolypeptides obtained from oriented fibers (see text), along with the corresponding 2-D images. Fiber orientation is along the vertical direction. In the copolymer spectra, the (10) and (01) reflections from the hexagonal and orthorhombic unit cells, remain intact independent from block composition.

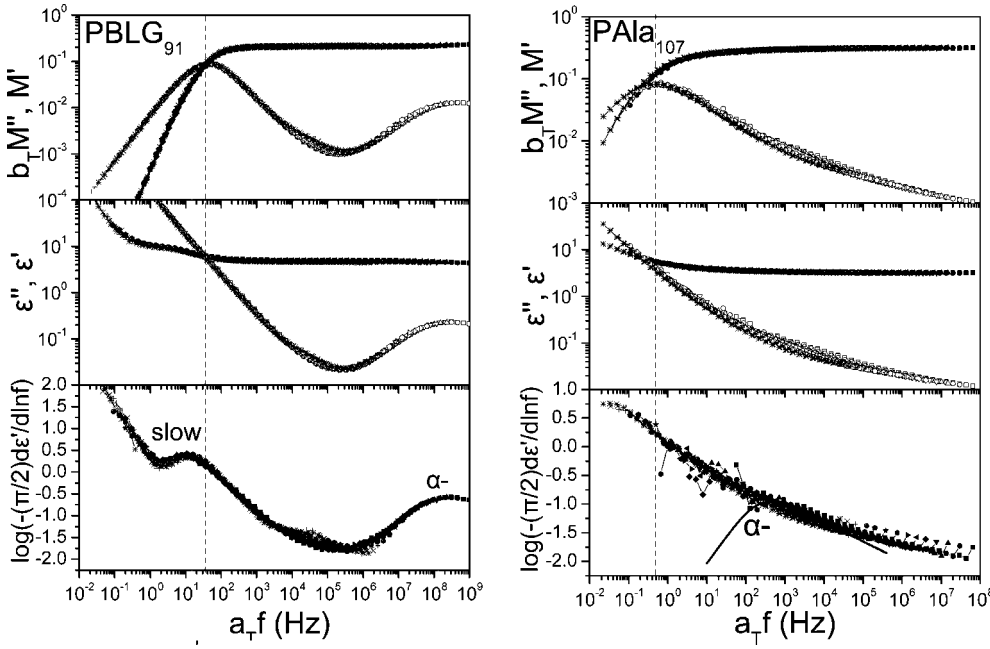

Figure 4. Superposition of the real and the imaginary parts of the electric modulus, M*, and of the complex dielectric permittivity, ϵ*, for the homopolypeptides at a reference temperature of 413 and 473 K, in the range 338 − 413 and 408 − 473 K for **PBLG$_{91}$** and **PAla$_{107}$**, respectively. The dashed lines indicate the crossing point of the real and imaginary parts. In **PBLG$_{91}$**, the segmental (α-), intermediate, and "slow" processes are observed, by increasing temperature order. On the other hand, the **PAla$_{107}$** α-process lies at very high temperature and can only be observed as a shoulder in the dielectric spectra.

In the copolymers, two C_α resonances are present, at 57.5 ppm and 53.1 ppm, revealing that both blocks form solely α-helical structures. This is clearly the case in the **PBLG$_{104}$-*b*-PAla$_{24}$** and **PBLG$_{115}$-*b*-PAla$_{48}$** copolymers but in the case of the **PBLG$_{105}$-*b*-PAla$_{79}$** (w_{PAla} = 21%) a small fraction of β-sheets (estimated to below 5%) cannot be totally excluded (shoulder at 48 ppm). Nevertheless, there is a suppression of the **PAla** β-sheet secondary structure in the copolypeptides that suggests a strong influence of chain topology on PAla conformations (see below). It is thought that this is the result of the thermodynamic field created by the enthalpic interactions of the unlike blocks. As we will see below, the same thermodynamic field is responsible for changes in the α-helical motifs as well. At present, the details of the mechanism (breaking of hydrogen bonds, time scales and possible kinetics) involved in these changes is not known.

Wide-angle X-ray measurements can provide both the peptide secondary structure and the unit cell in crystalline materials. Some representative WAXS images for the homopolypeptides are shown in Figure 3a. The diffraction pattern of **PBLG$_{45}$** exhibits a set of strong equatorial reflections together with some layer lines. The positions of the lines suggest an α-helical conformation of 18 residues in 5 turns (18/5 helix) with a repeat unit of c = 2.7 nm. This structure is described in the literature

as the paracrystalline form C; a nematic-like paracrystal with a periodic packing of α-helices in the direction lateral to the chain axis.[9] The strong equatorial **PBLG$_{45}$** reflections with ratios $1:3^{1/2}:4^{1/2}:7^{1/2}$, indicated with arrows, correspond to the 10, 01, 11 and 20 reflections of a hexagonal unit cell, with lattice parameter $\alpha = 1.51$ nm, and *d*-spacing given by

$$d_{hex} = \frac{1}{\sqrt{\frac{4}{3a^2}(h^2 + k^2 + hk)}} \quad (4)$$

where *h* and *k* are the Miller indices.

PAla$_{107}$ on the other hand forms both α-helices and β-sheets as revealed by the present NMR study. Earlier X-ray studies[30,41] of stretched fibers, swollen with dichloracetic acid, revealed a highly oriented and crystalline α-helical phase and a smaller amount of a highly oriented and crystalline β-form. The reflections from the α-helical form could be indexed on a unit cell with parameters $a = b = 0.855$ nm, $c = 7.0$ nm and $\gamma = 120°$. The unit cell contained 47 alanine residues and the *c*-axis periodicity corresponded to 13 turns giving rise to a 47/13 helix (pitch of 0.54 nm, axial translation per residue of 0.149 nm). Both left- and right-handed helices were examined. Later refinement[41] suggested a unit cell composed of "up" and "down" helices with a mutual displacement along the fiber axis. On the other hand, the reflections from the crystalline β-form could be indexed on a two-chain centered orthogonal cell with $a = 0.48$ nm, $b = 1.07$ nm, and $c = 0.69$ nm.

The powder **PAla$_{107}$** sample employed in the present study exhibits only some diffraction peaks at wave vectors 8.17, 11.6, 14.2, and 16.3 nm^{-1}, in the absence of long-range order. These reflections can be indexed using a simple two-dimensional model of an orthorhombic unit cell with a *d*-spacing given by

$$d = \frac{1}{\sqrt{\frac{h^2}{a^2} + \frac{k^2}{b^2}}} \quad (5)$$

with α=0.77 nm and *b*=0.55 nm. In Figure 3, the arrows correspond to the 01, 11, 02, and 12 reflections of the unit cell.

In the case of the copolypeptides, both the 10 and 01 reflections from the respective hexagonal and orthorhombic unit cells of PBLG and PAla, are present, in the 2-D WAXS images (Figure 3b). The corresponding PBLG and PAla unit cell parameters display insensitivity to PAla content. This suggests nanophase separation between the unlike blocks. However, the WAXS peaks are very broad and the correlation length, ($\xi \sim 2\pi/\Delta w$), obtained from the width (Δw) of the 10 and 02 reflections of PBLG and PAla, respectively, decreases significantly in the copolypeptides. Furthermore, the overlapping higher order PBLG reflections with the primary and higher order PAla reflections preclude the assignment of the type of peptide secondary structure in PAla. The ^{13}C NMR study better serves this purpose and clearly identifies the type of peptide secondary structure in the copolypeptides from the distinctly different chemical shifts. In summary, the NMR and X-ray studies reveal the presence of α-helical secondary structures corresponding to both PBLG and PAla segments, and in the PBLG case, X-rays further identify hexagonally packed α-helices. Furthermore, the insensitivity of the PBLG and PAla lattice parameters to composition suggests nanophase separation between the unlike blocks. This, however, could not be directly shown due to the low electron density contrast in small-angle X-ray scattering.

PBLG Dynamics. Superimposed dielectric loss curves for the two homopolypeptides are shown in Figure 4 at temperatures above the respective glass transitions. Two different representations are shown: the electric modulus *M** and the complex dielectric permittivity ε*, including the conductivity-free derivative of ε′. For **PBLG$_{91}$**, the data have been superimposed with respect to a reference temperature of 413 K. Starting from the high frequency side, the calculated dielectric loss spectra display the α-process followed by the weak "intermediate" process and by the intense "slow" process. As described previously in the literature,[8−10] the α-process originates from the relaxation of amorphous parts of the chain created by broken hydrogen bonds and from the chain-ends, the weak "intermediate" process reflects Rouse-type dynamics of completely amorphous chains and the slower process reflects the dynamics of the peptide secondary structure in its α-helical conformation. We mention here that polypeptides in their α-helical conformation can be considered as ideal examples of type-A polymers according to Stockmayers' classification[42] (i.e., bearing dipoles along the backbone) and the intensity of the slower process can be effectively used to calculate the persistence length (ξ) of the α-helical structures.

Important information on the side- and backbone dynamics in PBLG can be obtained by following the temperature dependence of the ^{13}C NMR spectra (Figure 5). **PBLG$_{91}$** forms solely α-helices as indicated by the C_α peak at $\delta \sim 58$ ppm and the amide C═O resonance ($\delta_3 \sim 176$ ppm). Resonances at $\delta_1 \sim 67$ ppm, $\delta_2 \sim 129$ ppm, and $\delta_4 \sim 172$ ppm correspond to the OCH_2, phenyl and side-group ester carbons, respectively, are indicated in the Figure. In the same Figure the temperature dependence of the peak intensities corresponding to the above resonances is compared. There is a general trend of decreasing peak intensity with increasing temperature. On top of that, a minimum can be observed that is more pronounced for the phenyl the OCH_2 resonances and even the C_β and C_γ resonances at 26.0 and 31.5, respectively. The intensity losses occur, because the local dynamics interferes with the magic angle spinning, cross polarization, and dipolar decoupling all of order 20 kHz or so.[43] The arrows in the Figure indicate the temperatures where the intensity is minimized suggesting rates of the underlying molecular motions at the NMR frequency ($\omega = 2\pi f, f = 20$ kHz). Notice that the faster molecular motion is that of the phenyl ring followed by the somewhat slower dynamics of the OCH_2 and side ester groups. Nevertheless, the temperature difference between these resonances is below 10 K, so for practical purposes we can assume that the side group relaxes as a whole. At these temperatures the backbone remains immobile (amide C═O resonance at δ_3=176 ppm) on the time scale introduced above, suggesting a decoupling for the side-group from the backbone dynamics. The backbone gains some mobility only at higher temperatures (estimated at T∼380 K) at the NMR frequency.

On the basis of the combined information from DS and ^{13}C NMR experiments on the motional rates and the geometry of motion at the single NMR frequency, respectively, a comparison of the relaxation times can be made and the outcome is shown in Figure 6. In the Figure the relaxation times corresponding to the β-process obtained from DS show Arrhenius temperature dependence

$$\tau_{max} = \tau_0 \exp\left(\frac{E}{RT}\right) \quad (6)$$

where $\tau_0 \sim 10^{-14}$ s and *E* is the apparent activation energy (52 ± 1 kJ/mol). On the other hand the α-process displays the usual strong temperature dependence that conforms to the Vogel−Fulcher−Tammann (VFT) equation as

$$\tau_{max} = \tau_0 \exp\frac{D_T T_0}{T - T_0} \quad (7)$$

where $\tau_0 = (5.0 \pm 0.5) \times 10^{-12}$ s, D_T (=5.5 ± 0.2) is a dimensionless parameter and T_0 (=241 ± 1) is the "ideal" glass temperature. The "slower" process associated with the dynamics

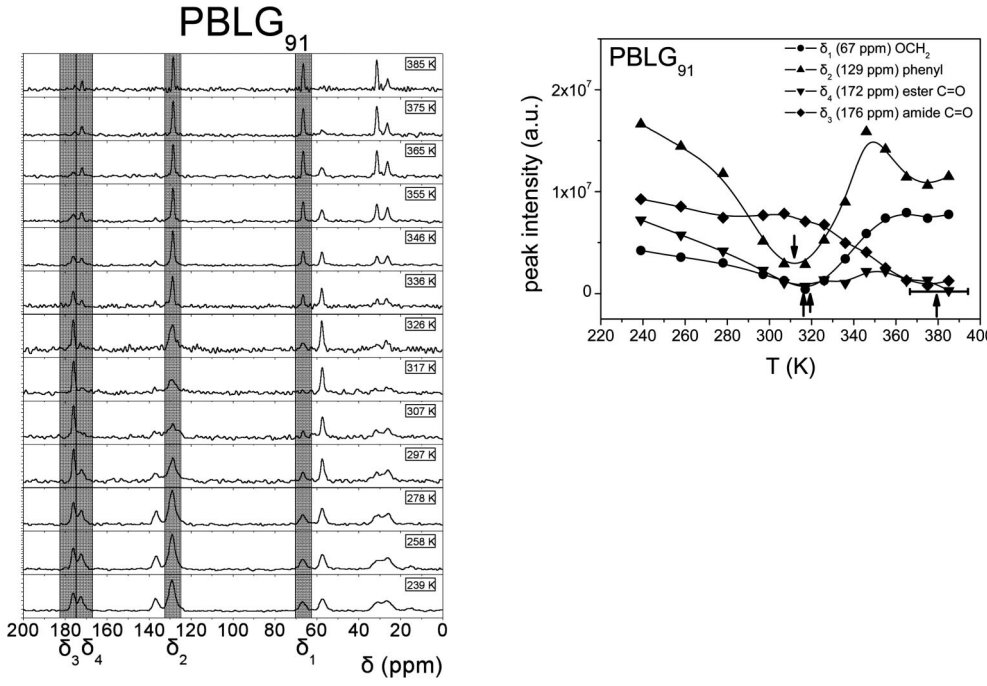

Figure 5. (Left) ^{13}C NMR spectra of **PBLG$_{91}$** as a function of temperature. Resonances at $\delta_1 \sim 67$ ppm, $\delta_2 \sim 129$ ppm and $\delta_4 \sim 172$ ppm correspond to the OCH_2, phenyl and side-group ester carbons, respectively. (Right) Temperature dependence of the peak intensities corresponding to the above resonances. The arrows indicate the temperatures where the intensity is minimized suggesting resonances of the underlying molecular motions at the NMR frequency ($\omega = 2\pi f$, $f = 20$ kHz). Notice that the faster molecular motion is that of the phenyl ring followed by the somewhat slower dynamics of the OCH_2 and side ester groups.

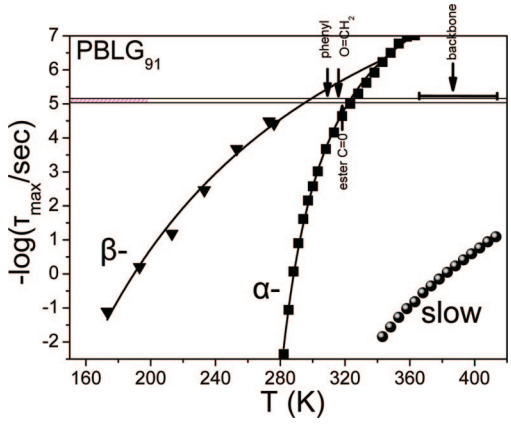

Figure 6. Relaxation times for the Arrhenius β- (triangles) and α-processes (squares) and the "slower" process (spheres) of **PBLG$_{91}$**, obtained from DS, plotted as a function of temperature. The solid lines are fits to an Arrhenius and VFT equations for the β- and α-processes, respectively. The ^{13}C NMR resonances from Figure 5 are indicated with arrows at the corresponding NMR frequency.

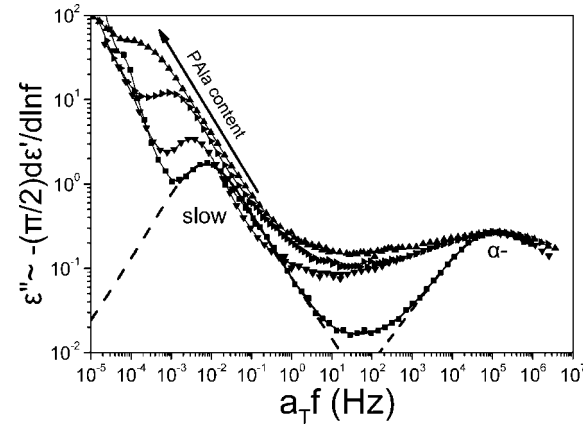

Figure 7. Superimposed ε''_{der} spectra at 333 and 415 K (calculated with the aid of the derivative method) plotted at a reference temperature of 333 K. The spectra display the faster α-process associated with the dynamic glass temperature of the PBLG block and a slower process associated with the relaxation of the α-helical secondary structure; **PBLG$_{91}$** (squares), **PBLG$_{104}$-*b*-PAla$_{24}$** (down triangles), **PBLG$_{115}$-*b*-PAla$_{48}$** (right triangles), **PBLG$_{105}$-*b*-PAla$_{79}$** (up triangles). The dashed lines represent examples of fits to two HN equations corresponding to the α- and slower processes. Notice that the α-process broadens with increasing PAla content in the copolymers, whereas the slower process shifts to lower frequencies and intensifies with increasing PAla content. The latter suggests the partial annihilation of PBLG α-helical defects with increasing PAla content.

of the α-helical segments are also included in the Figure. Clearly, the collective dynamics of α-helical segments are orders of magnitude slower than the local segmental dynamics within the amorphous defected regions. The ^{13}C NMR resonances from Figure 5 are indicated with arrows at the NMR frequency. Notice that the phenyl, the OCH_2 and side group ester dynamics are located in the vicinity of the merging of the α- and β-processes. Since the motion of the phenyl group itself is dielectrically inactive we conclude that the β-process, as probed dielectrically, likely, reflects the ester C═O and OCH_2 dynamics. Backbone motions, as probed by NMR, start at higher temperatures than the DS segmental α-process. This is conceivable since DS is sensitive to the backbone dynamics within the "defected" amorphous regions, which unfortunately do not show up in our NMR spectra. They are dominated by the signals of the α-helices. Therefore, NMR probes the backbone dynamics within the α-helical segments (for example, through the amide C═O resonance), or in general, in more ordered regions. On the other hand, the backbone dynamics as probed by NMR are considerably faster than the DS "slow" process associated with the complete relaxation of α-helices bearing the larger dipoles. This suggests a low amplitude backbone motion as seen in the NMR experiment through the amide C═O resonance. This is substantiated by the fact that this motion leaves the side-chain unaffected (i.e., nearly constant intensities of the OCH_2 and phenyl resonances at the higher

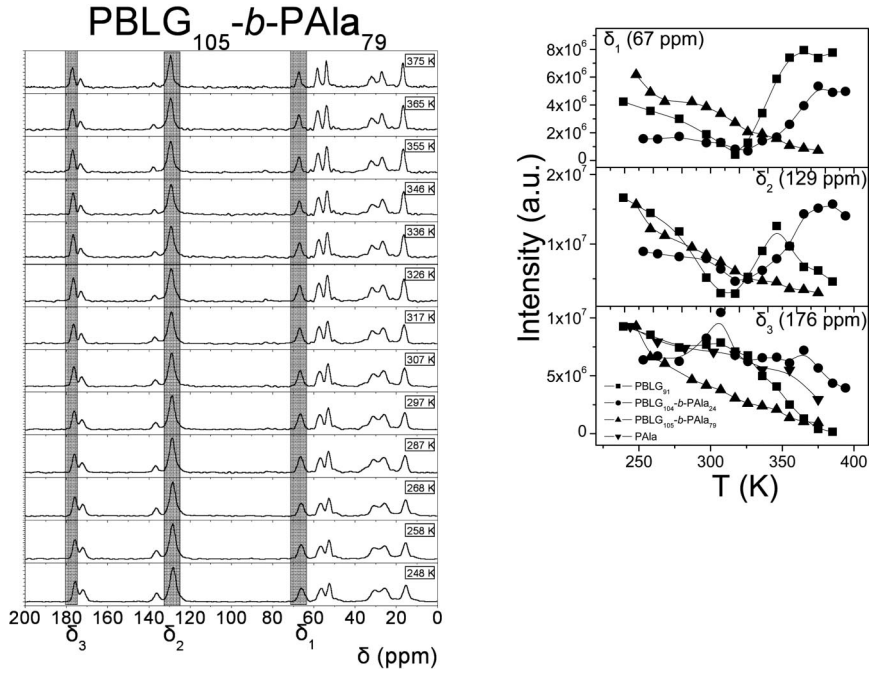

Figure 8. (left) ^{13}C NMR spectra of the **PBLG$_{105}$-*b*-PAla$_{79}$** diblock as a function of temperature. Both blocks form α-helices as indicated by the peaks at $\delta \sim 57.5$ ppm and $\delta \sim 53.1$ ppm corresponding to PBLG and PAla C_a resonances, respectively. Resonances at $\delta_1 \sim 67$ ppm, $\delta_2 \sim 129$ ppm and $\delta_3 \sim 176$ ppm correspond to the OCH_2, phenyl and amide C═O ester carbons, respectively. (right) Temperature dependence of the peak intensities corresponding to the above resonances for the bulk PBLG (squares), PAla (down triangles) and two diblocks, **PBLG$_{104}$-*b*-PAla$_{24}$** (circles) and **PBLG$_{105}$-*b*-PAla$_{79}$** (up triangles).

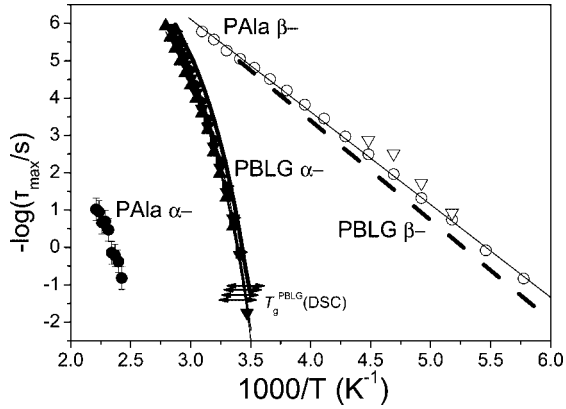

Figure 9. Arrhenius relaxation map of the segmental (α-) processes in the homopolypeptides and the copolypeptides. The α- and β- processes of bulk **PBLG** are shown with solid and dashed lines respectively, whereas the corresponding processes for **PAla** are shown with filled and open circles. The α-process in the copolypeptides is shown with the following symbols: **PBLG$_{104}$-*b*-PAla$_{24}$** (down triangles), **PBLG$_{115}$-*b*-PAla$_{48}$** (right triangles), **PBLG$_{105}$-*b*-PAla$_{79}$** (up triangles). Lines are fits to the VFT (α-process) or the Arrhenius equation (β-process). The DSC T_g corresponding to the PBLG block in the copolymers is indicated with arrows at $\tau \sim 10$ s.

temperatures investigated). Therefore, the NMR process can be considered as a precursor to the unfreezing of the helical dynamics probed dielectrically. This process does not manifest itself as a separate process in DS for intensity reasons (i.e., very low amplitude motion).

Copolymer Dynamics. At this point it would be interesting to explore the consequences of the structural changes found by NMR (on the peptide secondary structure) and X-ray scattering (nanophase separation) on the polypeptide dynamics. In Figure 7, we compare the PBLG and the copolymer dielectric loss spectra obtained from the derivative of the dielectric permittivity spectra at 333 and 415 K shifted to the 333 K spectrum. In the copolypeptides, the PBLG α-process remains practically at the same frequency and is significantly broadened. Additionally, the "slow" process, associated with the relaxation of α-helical segments, is more intense and shifts to lower frequencies as compared to the corresponding process in bulk PBLG. The "slow" process in the copolypeptides can only originate from the relaxation of the PBLG secondary structure, since the respective slow process in PAla would be observed at much higher temperatures/lower frequencies. Although the deconvolution of this "slow" process from the overlapping dc conductivity is difficult, it can be deduced that its dielectric intensity is higher than that of the pure PBLG. The effective dipole moment responsible for the relaxation of the α-helical segments can be estimated with the use of the Buckingham equation[44] (modified by Applequist and Mahr) suitable for rigid-rod molecules

$$\frac{Nfg\mu^2}{3\varepsilon_0 k_B T} = \frac{(2\varepsilon_s + 1)(\varepsilon_s - n^2)}{2\varepsilon_s + n^2} - \frac{(2\varepsilon_\infty + 1)(\varepsilon_\infty - n^2)}{2\varepsilon_\infty + n^2} \quad (8)$$

where N is the number density of dipoles (in the calculation we have used for the mass density 1.278 g/cm^3 for PBLG), μ is the dipole moment, f and g are factors related to the geometry of the molecule ($f \rightarrow {}^2/_3$ and $g \rightarrow 1$ for an infinitely long rod), ϵ_s and ϵ_∞ are the unrelaxed and relaxed components of the permittivity for the process under investigation and n is the refractive index. The thus obtained effective dipole moments μ_{eff} $(= g^*\mu^2)^{1/2}$, where g^* is the Kirkwood−Fröhlich pair correlation factor between neighboring dipoles, is 20 D which is higher than in bulk PBLG of the same molecular weight. This implies *partial* annihilation of the α-helical defects in the copolymers because of the thermodynamic field as in PBLG-*b*-poly(dimethyl siloxane)-*b*-PBLG triblock copolymers.[22] Nevertheless, the estimated effective dipole moments for the PBLG α-helical segments in the copolypeptides are still far from an "ideal" PBLG α-helix (~20 D as compared to 200 D for the same degree of polymerization).

We now return to the geometry of the motions and we thus refer to the ^{13}C NMR results of the copolymers. All copolypep-

Table 2. VFT Parameters and T_g of the PBLG Phase in the Copolymers

compound	$-\log(\tau_0/s)$	D_T	T_o (PBLG) (K)	T_g^{DS}(PBLG) (K)	T_g^{DSC}(PBLG) (K)
$PBLG_{91}$	11.3 ± 0.2	5.5 ± 0.2	241 ± 1	284 ± 1	286 ± 15
$PBLG_{104}$-*b*-$PAla_{24}$	11.3 ± 0.5	6.1 ± 0.8	239 ± 4	286 ± 4	293 ± 20
$PBLG_{115}$-*b*-$PAla_{48}$	12.5 ± 0.2	8.1 ± 0.4	229 ± 2	286 ± 2	301 ± 50
$PBLG_{105}$-*b*-$PAla_{79}$	12.4 ± 0.4	9.1 ± 0.9	225 ± 4	287 ± 4	305 ± 50

tides were studied by ^{13}C NMR and representative spectra of the **$PBLG_{105}$-*b*-$PAla_{79}$** diblock as a function of temperature are depicted in Figure 8. As we discussed earlier, both blocks form α-helices as indicated by the peaks at $\delta \sim 57.5$ ppm and $\delta \sim 53.1$ ppm corresponding to PBLG and PAla C_a resonances, respectively. Resonances at $\delta_1 \sim 67$ ppm, $\delta_2 \sim 129$ ppm and $\delta_3 \sim 176$ ppm corresponding to the OCH_2, phenyl and amide C═O ester carbons, respectively, are indicated in the Figure. In the same figure the temperature dependence of the peak intensities corresponding to the above resonances for the homopolypeptides and two of the diblocks **$PBLG_{104}$-*b*-$PAla_{24}$** and **$PBLG_{105}$-*b*-$PAla_{79}$** are shown (the third is omitted for clarity). Notice that the intensity minima corresponding to the phenyl (δ_2) and OCH_2 (δ_1) resonances are still present in the copolymers with the higher PBLG content (**$PBLG_{104}$-*b*-$PAla_{24}$**) but is absent in the diblock with the lower PBLG content (**$PBLG_{105}$-*b*-$PAla_{79}$**) suggesting a more rigid structure. Thus increasing PAla content in the diblocks, results in a dynamically rigidified PBLG side-group motion. Thus the observation that the PBLG β-process will likewise be suppressed in the copolymers with the higher PAla content is borne out by the ^{13}C NMR results.

The local segmental and sub-T_g dynamic processes in the homopolypeptides and the copolypeptides are compared in Figure 9 in the usual Arrhenius representation. The PAla β-process with $\tau_0 \sim 10^{-14}$ s, $E = 47.7 \pm 0.4$ kJ/mol, with a distribution of relaxation times as given by $m = 0.4$, $n = 0.75$ and a dielectric strength $T\Delta\epsilon \sim 25$ K, lies in the vicinity of the corresponding process of PBLG. The latter is characterized by $\tau_0 \sim 10^{-14}$ s, $E = 52 \pm 1$ kJ/mol, $m = mn = 0.45$ and a lower dielectric strength $T\Delta\epsilon \sim 5$ K. Despite the proximity of the β-process motional rates their origin must be very different; in PBLG the combined ^{13}C NMR and DS results suggest the relaxation of the side-group bearing the OCH_2 and C═O ester as responsible for the β-process. Yet the side chain of PAla does not have a dipole; hence this relaxation must reflect the low amplitude motion of the PAla backbone. In the copolypeptides, it is only in the **$PBLG_{104}$-*b*-$PAla_{24}$** that a β-process is evident. This process is assigned to PBLG due to its lower dielectric strength ($T\Delta\epsilon$ 5 ~ K). The suppression of the PBLG β-process in the remaining copolypeptides is in agreement with the ^{13}C NMR result, namely, that the side group motion is suppressed in the copolymers with the higher PAla content.

The segmental processes of the homopolypeptides are shown also in Figure 9. The α-process of PAla is weak in DS (Figure 4), nevertheless the estimated relaxation times are included in the Figure. The PBLG segmental process in the copolypeptides, is nearly identical to bulk PBLG with the same strong temperature dependence and nearly the same VFT parameters (Table 2). This insensitivity of the PBLG α-relaxation times to composition confirms the nanophase separation between unlike segments.

The combined information from the structural and dynamic probes allows constructing a realistic model of the dynamic structure in the copolypeptides that is shown in Figure 10. The schematic depicts nanophase separated PBLG and PAla domains based on the structural (X-ray) and dynamic investigation (DS). The respective domains consist of PBLG and helices (NMR) that are hexagonally packed (WAXS) and further interrupted by amorphous segments created by broken hydrogen bonds (DS). It is the dipolar dynamics within these domains that give rise to the dielectric α-process. The effect of thermodynamic confinement is to make the PBLG α-helices in the copolypeptides more persistent as compared to bulk PBLG (DS). Yet they still contain amorphous defects (i.e., "defected" helices).

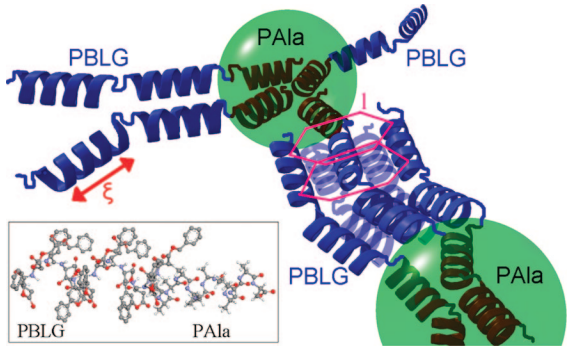

Figure 10. Highly schematic representation of the copolymer self-assembly showing PBLG and PAla α-helices (NMR, WAXS) that are hexagonally packed (WAXS). The persistence of the PBLG α-helices (ξ) is obtained through DS. In the inset, a schematic of a $PBLG_{12}$-*b*-$PAla_{12}$ diblock copolymer is shown in the "ideal" fully extended conformation (red, O; blue, N; gray, C).

Conclusions

The systematic investigation of the self-assembly and dynamics of a series of copolypeptides composed of PBLG and PALa blocks revealed strong effects of the thermodynamic field on the peptide secondary structures. Although pure PAla stabilizes both α-helices and β-sheets, in the copolypeptides the latter motif was suppressed. This suggested that the PAla β-sheets are less stable than α-helices and hence more prone to the thermodynamic restrictions imposed by the copolymers. In addition, the effect of the thermodynamic field on the α-helical secondary motif of PBLG is to annihilate some of the amorphous structural defects. This effectively increases the persistence length of α-helices.

The PBLG dynamics were followed both below and above the glass temperature. A hierarchy of motions was unraveled from the local β-process, to the segmental α-process and to slower processes associated with the backbone dynamics within the α-helical motif by a combination of NMR and DS. The dielectrically active β-process reflects the side-chain dynamics whereas the α-process the segmental dynamics within the amorphous "defected" domains. Thus, NMR and DS provide much more information on the backbone motion than either of them alone as they probe different aspects of the backbone dynamics; the former being sensitive to the low-amplitude restricted backbone dynamics and the latter to the complete relaxation of α-helical segments. In this respect, the low-amplitude backbone dynamics is a precursor of the relaxation of the secondary structure.

Overall these results suggest a way to manipulate the type and persistence of peptide secondary structures through the thermodynamic confinement in block copolypeptides. Despite the strong effects on the peptide secondary structures, the exact mechanism, especially behind the destabilization of β-sheets, is unknown.

Acknowledgment. This work was cofinanced by the E.U.-European Social Fund (75%) and the Greek Ministry of Development-GSRT (25%) in the framework of the program PENED2003 (No 856). We thank A. Best, M. Bach (MPI-P), and G. Tsoumanis (UoI) for technical support. Financial support of the Deutsche Forschungsgemeinschaft, SFB 625, is gratefully acknowledged.

References and Notes

(1) Kricheldorf, H. R. *Angew. Chem., Int. Ed.* **2006**, *45*, 5752.
(2) Klok, H.-A.; Lecommandoux, S. *Adv. Polym. Sci.* **2006**, *202*, 75.
(3) Hol, W. G. J.; van Duijnen, P. T.; Berendsen, H. J. C. *Nature* **1978**, *273*, 443.
(4) Feng, J. A.; Tessler, L. A.; Marshall, G. R. *Int. J. Peptide Res. Therapeutics* **2007**, *13*, 151.
(5) Oommachen, S.; Ren, J.; McCallum, C. M. *J. Phys. Chem. B* **2008**, *112*, 5702.
(6) Walton, A. G.; Blackwell, J. *Biopolymers*; Academic Press: New York, 1973.
(7) Block, H. *Poly(γ-benzyl-L-glutamate) and other glutamic acid containing polymers*; Gordon and Breach Science Publishers: New York, 1983.
(8) Floudas, G.; Papadopoulos, P.; Klok, H.-A.; Vandermeulen, G. W. M.; Rodriguez-Hernandez, J. *Macromolecules* **2003**, *36*, 3673.
(9) Papadopoulos, P.; Floudas, G.; Klok, H.-A.; Schnell, I.; Pakula, T. *Biomacromolecules* **2004**, *5*, 81.
(10) Papadopoulos, P.; Floudas, G.; Schnell, I.; Klok, H.-A.; Aliferis, T.; Iatrou, H.; Hadjichristidis, N. *J. Chem. Phys.* **2005**, *122*, 224906.
(11) Blondelle, S. E.; Forood, B.; Houghten, R. A.; Pérez-Payá, E. *Biochemistry* **1997**, *36*, 8393.
(12) Asakura, T.; Yang, M.; Kawase, T.; Nakazawa, Y. *Macromolecules* **2005**, *38*, 3356.
(13) Sarikaya, M.; Tamerler, C.; Jen, A. K.-Y.; Schulten, K.; Baneyx, F. *Nat. Mater.* **2003**, *2*, 577.
(14) Deming, T. J. *Nature* **1997**, *390*, 386.
(15) Aliferis, T.; Iatrou, H.; Hadjichristidis, N. *Biomacromolecules* **2004**, *5*, 1653.
(16) Lecommandoux, S.; Achard, M.-F.; Langenwalter, J. F.; Klok, H.-A. *Macromolecules* **2001**, *34*, 9100.
(17) Douy, A.; Gallot, B. *Polymer* **1982**, *23*, 1039.
(18) Klok, H.-A.; Langenwalter, J. F.; Lecommandoux, S. *Macromolecules* **2000**, *33*, 7819.
(19) Schlaad, H.; Antonietti, M. *Eur. Phys. J. E* **2003**, *10*, 17.
(20) Schlaad, H.; Smarsly, B.; Losik, M. *Macromolecules* **2004**, *37*, 2210.
(21) Papadopoulos, P.; Floudas, G.; Schnell, I.; Aliferis, T.; Iatrou, H.; Hadjichristidis, N. *Biomacromolecules* **2005**, *6*, 2352.
(22) Papadopoulos, P.; Floudas, G.; Schnell, I.; Lieberwirth, I.; Nguyen, T. Q.; Klok, H.-A. *Biomacromolecules* **2006**, *7*, 618.
(23) Gitsas, A.; Floudas, G.; Dietz, M.; Mondeshki, M.; Spiess, H. W.; Wegner, G. *Macromolecules* **2007**, *40*, 8311.
(24) Duncan, R. *Nat. Rev. Drug Discovery* **2003**, *2*, 347.
(25) Koynov, K.; Mihov, G.; Mondeshki, M.; Moon, C.; Spiess, H. W.; Müllen, K.; Butt, H.-J.; Floudas, G. *Biomacromolecules* **2007**, *8*, 1745.
(26) Mondeshki, M.; Mihov, G.; Graf, R.; Spiess, H. W.; Müllen, K.; Papadopoulos, P.; Gitsas, A.; Floudas, G. *Macromolecules* **2006**, *39*, 9605.
(27) Babin, J.; Taton, D.; Brinkmann, M.; Lecommandoux, S. *Macromolecules* **2008**, *41*, 1384.
(28) Gitsas, A.; Floudas, G.; Mondeshki, M.; Spiess, H. W.; Iatrou, H.; Hadjichristidis, N. *Biomacromolecules* **2008**, *9*, 1959.
(29) Chen, M. C.; Lord, R. C. *J. Am. Chem. Soc.* **1974**, *96*, 4750.
(30) Brown, L.; Trotter, I. F. *Trans. Faraday Soc.* **1956**, *52*, 537.
(31) Lee, D.-K.; Ramamoorthy, A. *J. Phys. Chem.* **1999**, *103*, 271.
(32) Aliferis, T.; Iatrou, H.; Hadjichristidis, N. *Biomacromolecules* **2004**, *5*, 1653.
(33) Poché, D.; Moore, M. J.; Bowles, J. L. *Synth. Commun.* **1999**, *29*, 843.
(34) Langer, B.; Schnell, I.; Spiess, H. W.; Grimmer, A.-R. *J. Magn. Reson.* **1999**, *138*, 182.
(35) Metz, G.; Wu, X.; Smith, S. O. *J. Magn. Reson.* **1994**, *110*, 219.
(36) Bennett, A. E.; Rienstra, C. M.; Auger, M.; Lakshmi, K. V.; Griffin, R. G. *J. Chem. Phys.* **1995**, *103*, 6951.
(37) Fischbach, I.; Pakula, T.; Minkin, P.; Fechtenkötter, A.; Müllen, K.; Spiess, H. W.; Saalwächter, K. *J. Phys. Chem. B* **2002**, *106*, 6408.
(38) Floudas, G. In *Broadband Dielectric Spectroscopy*; Kremer, F., Schönhals, A. Eds, Springer: Berlin, 2002; Chapter 8.
(39) Havriliak, S.; Negami, S. *Polymer* **1967**, *8*, 161.
(40) Saito, H.; Tabeta, R.; Shoji, A.; Ozaki, T.; Ando, I. *Macromolecules* **1983**, *16*, 1050.
(41) Arnott, S.; Wonacott, A. J. *J. Mol. Biol.* **1966**, *21*, 371.
(42) Stockmayer, W. H. *Pure Appl. Chem.* **1967**, *15*, 539.
(43) Rothwell, W.; Waugh, J. S. *J. Chem. Phys.* **1981**, *74*, 2721.
(44) Buckingham, A. D. *Aust. J. Chem.* **1953**, *6*, 323.

MA801770B